Lee-wave breaking over obstacles in stratified flow

Olivier S. Eiff[a)]
Météo-France, Centre National de Recherches Météorologiques, 42 av Coriolis, 31057 Toulouse, France and Institut de Mécanique des Fluides de Toulouse, Allée du Professeur Camille Soula, 31400 Toulouse, France

Philippe Bonneton
Université Bordeaux I, Département de Géologie et Océanographie, 33405 Talence, France

(Received 26 January; accepted 23 December 1999)

Experimental results are presented on the lee-wave breaking process which occurs at low Froude numbers when uniform and strongly stratified flow approaches two-dimensional and quasi two-dimensional Gaussian-shaped obstacles. It was found that the lee-wave breaking process is essentially independent of the two-dimensional and the quasi two-dimensional shape of the obstacles. The attainment of the critical condition where the steepening wave becomes statically unstable does not mark a threshold to breakdown. Instead, the wave remains dynamically stable for several buoyancy periods, overturning into an ''S''-shape with maximum overturning reaching about 55° past the vertical. It is observed that the primary instability forms a quasi two-dimensional spanwise vortex over the central portion of the obstacles and is mainly shear driven. The quasi two-dimensional spanwise vortex persists for a few buoyancy periods before undergoing a three-dimensional convective instability, similar to a Rayleigh–Taylor instability. As a result, an array of toroidal vortex structures aligned parallel to the obstacle crest forms. These vortex structures of size $\sim 3H$ are inclined into the flow yielding three strong components of vorticity.
 [S1070-6631(00)01604-4]

I. INTRODUCTION

The flow of uniformly stratified fluid over an obstacle such as a mountain can lead to stationary lee-waves. Long[1,2] developed a nonlinear stationary two-dimensional model for these flows and showed that for sufficiently small obstacles it was in remarkable agreement with laboratory experiments. Clark and Peltier,[3] Peltier and Clark,[4] and Laprise and Peltier[5] demonstrated, from numerical simulations of unbounded flows, that when the Froude number F ($F=U/NH$, where U is the upstream velocity, H is the obstacle height and $N=(-g/\rho_0\ d\rho/dz)^{1/2}$ is the Brunt–Väisälä frequency) is below the critical value, F_c, for which the streamlines overturn locally in Long's steady-state solution, the lee-wave becomes statically unstable and undergoes a transition. The flow changes from a freely propagating internal wave flow, well described by Long's model, to a different configuration with a region of intense turbulence and a strong acceleration of the low-level flow in the lee of the obstacle. This phenomenon is particularly important in the meteorological context, because it is responsible for downslope windstorms occurring on the lee-side of mountain ranges such as the Rocky mountains.[6] Lee-wave breaking is also responsible for a further increase in drag imparted on the atmosphere, which needs to be accounted for in numerical weather prediction models.

Theoretical investigations of the lee-wave breaking phenomenon have been done essentially in Long's inviscid context. Smith[7] developed a nonlinear hydrostatic theory to predict the vertical location of the breaking region and the associated increase of the wind speed and drag. Laprise and Peltier[8] have undertaken the two-dimensional linear stability analysis of Long's steady-state nonlinear solution. They showed that for $F<F_c$, in addition to a local convective mode, the dominant instability mechanism is of a shear-flow type which feeds on the shear layer between the steepening wave level and the ground. The more recent three-dimensional simulations by Afanasyev and Peltier,[9] suggest that the instability behavior is three-dimensional and similar to the shear-aligned convective instability described by Klassen and Peltier[10] in Kelvin–Helmholtz rolls. Further three-dimensional high-resolution simulations of gravity wave breaking near a critical level by Fritts and Isler,[11] Winters and D'Asaro,[12] and Andreassen *et al.*,[13] or of propagating internal-wave breaking by Lombard and Riley[14] also suggest that wave breaking is essentially dominated by three-dimensional instability in which both convective and shear effects can be important to varying degrees depending on the particular conditions of the flow.

Experimental studies focusing on lee-wave breaking such as those by Rottman and Smith[15] and Castro and Snyder[16] have undertaken systematic towing tank experiments to study the range of F leading to wave breaking for different obstacle shapes. These experiments mainly addressed the occurrence of wave breaking but did not describe the lee-wave breaking instability nor its evolving dominant large-scale structures.

Thus, it is the objective of the present paper to describe

a)Electronic mail: eiff@cnrm.meteo.fr

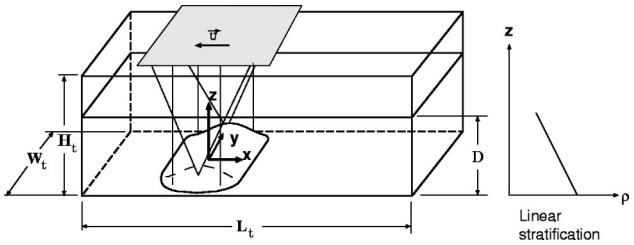

FIG. 1. Experimental setup.

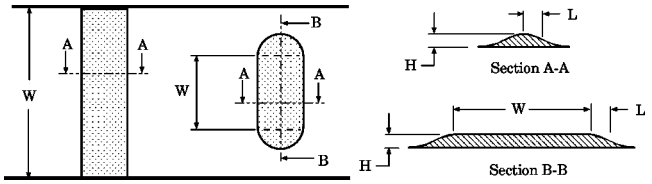

FIG. 2. Schematic of the two-dimensional and quasi-two dimensional obstacles.

new experimental results examining the three-dimensional features of the lee-wave breaking instability and the emerging large-scale vortex structures in the wave-breaking zone. In Sec. II, we describe the experimental facilities and procedures. Then, in Sec. III, we present some complementary results to the extensive study of Castro and Snyder[16] on the lee-wave regimes for two-dimensional Gaussian obstacles in order to situate the lee-wave breaking regime investigated in detail in the following sections. In particular, the process of lee-wave breaking is described in Sec. IV, beginning with an overview of the transient evolution (Sec. IV A) and followed by the observed primary (Sec. IV B) and secondary lee-wave instabilities (Sec. IV C). The three-dimensional nature of the emerging large-scale structures in the breaking zone is shown and discussed in Sec. V.

II. EXPERIMENT

The experiments were conducted in three different water towing-tanks of size $H_t \times W_t \times L_t$ equal to $0.5\times0.5\times4$ m^3(small tank), $0.7\times0.8\times7$ m^3 (medium tank) and $1.5\times3\times22$ m^3 (large tank), which allowed three different Reynolds number magnitudes to be examined. (See Fig. 1 for a sketch of the experimental set-up.) These Reynolds number magnitudes ($\mathrm{Re}=UH/\nu$, where U is the towing or freestream velocity and H is the obstacle height) were 10^2, 10^3, and 10^4 for the three tanks, respectively. Baines and Manins[17] suggest that Reynolds numbers exceeding several hundred are necessary in order to correctly model the large-scale turbulence as encountered in atmospheric flows. Thus, only the high Reynolds number range is expected to be characterized by fully turbulent conditions. Both the low and medium ranges, however, are still likely to yield the same fundamental large-scale motions, as will be shown.

Many experiments dealing with lee-waves in a stratified fluid had adopted a towing-carriage technique where the obstacle was mounted on a flat baseplate suspended from the carriage and towed upside-down across the stationary fluid (e.g., Hunt and Snyder[18]). To avoid the perturbations generated by the baseplate, we preferred an upright towing configuration in which the obstacles were towed tangentially along the bottom of the tank at uniform speed (U). In the upright configuration the Reynolds numbers associated with the supporting threads, ranging from 0.5 to 60, induce negligible downstream disturbances. The gap between the baseplate of the obstacle and the tank floor, less than about 0.1 H, also produces no significant flow perturbations, as confirmed by experiments using the small obstacles with increasing gap spacings which did not reveal flow perturbations up to 0.3 H.

The experiments were performed with two-dimensional and quasi two-dimensional Gaussian-shaped obstacles (see Fig. 2). The streamwise cross-sectional profiles for both types of obstacles are given by $h(x)=H\ \exp(-x^2/2L^2)$ with $H/L=0.57$. Based on the total length of the mountain, $2L_o$, the aspect ratio is $H/L_o=0.23$, corresponding to a gentle to moderate slope.[15] The two-dimensional obstacles, used in the small and medium tanks, are uniform across the entire spanwise direction, spanning the width of the tank except for a thin spacing of 2 mm at the walls. The quasi two-dimensional obstacles, used in all three tanks, were chosen to make the flow as two-dimensional as possible and yet minimize the upstream perturbations caused by flow blocking for $F<1$.[19] Thus, the quasi two-dimensional obstacles are also uniform along the spanwise direction, but the ends are smoothed by the same Gaussian shape as in the streamwise direction, in a semicircular manner. The quasi two-dimensional obstacles were scaled such that the spanwise aspect ratio (W/H) and confinement (W/W_t) in each tank were the same, specifically, $W/H=10.3$ and $W/W_t=0.45$. (Note that the latter ratio required a separating wall to be used in the small tank to adjust W_t to 0.37 m.) In the case of the two-dimensional obstacles, $W/H=31$ for the small tank and $W/H=24$ for the medium tank. The maximum perturbations due to upstream blocking and the resulting wall reflections are expected to be obtained with the two-dimensional obstacles as the end of tanks are approached (increasing Nt). In the small tank, measurements of the longitudinal velocity profile, taken 30 L ahead of the end-wall at the moment when the two-dimensional obstacle is approaching at a distance 40 L from the measurement location, showed that the maximum upstream perturbation is less than $0.1U$. This position of the obstacle relative to the end-wall corresponds to the highest nondimensional times reported here ($\mathrm{Nt}=150$).

The linear stratification (NaCl solution) was obtained by a computer-monitored filling process to yield Brunt–Väisälä frequencies, N, in the range of $N\in[0.8,1.1$ rad/s]. The linearity does not maintain itself at the bottom or at the top of the tank due to convective and diffusive effects at those boundaries. This can be expected to pose a problem in the case of the bottom layer where the waves are generated by the obstacles. However, tests with different thicknesses have revealed that the lee-wave dynamics are not affected when the bottom layer thickness does not exceed 0.6 H. Care was taken to ensure that this thickness was held well below this limit at 0.2 H. Subtracting the depth of the top layer, the effective vertical confinement (D) over which the stratifica-

tion is linear was about $D/H=8$ with a maximum root-mean square (rms) deviation of the linear density profile less than 0.2%. Tests with higher D/H ratios (up to 40) in the small tank did not reveal an influence of this ratio on the wave field in the lower lee-wave zone of interest.

The flow was examined via two basic techniques, fluorescent-dye and particle visualizations. In both techniques, a thin laser sheet is used to illuminate a cross-sectional plane of the flow which is filmed by CCD (charge coupled device) cameras and recorded on S-VHS tape for subsequent processing. In the fluorescent-dye visualizations, the dye was introduced into the flow by creating fixed vertical (xz) fluorescent-dye planes along the length of the tank. These planes were obtained by carefully pulling a vertical rake of thin cotton threads painted with fluorescent dye shortly before towing the obstacle. The fluorescent planes appear as lines in any given horizontal laser-illuminated plane. In the particle visualization technique, neutrally buoyant particles spanning the range of densities in the stratified fluid are seeded throughout the fluid well in advance of the tows. Their settling velocity is, therefore, effectively zero. Two methods to analyze the resulting particle recordings were used: Particle-tracking and particle image velocimetry (PIV) based on the cross-correlation of two images (TSI-Insight™). The flows were also examined in two planes simultaneously, either with particle-tracking in both planes or particle-tracking in one and fluorescent-dye in the other. This was realized by using two laser sheets of different frequencies in conjunction with appropriate optical filters mounted on the cameras.

For steady, incompressible flow, the pathlines obtained from a time-integration of the particle displacements in the particle tracking technique would be equivalent to streamlines and isopycnal lines. For the slowly evolving flows examined here, relatively short time integrations are used ($N\delta t=2$) such that the pathlines can nevertheless be considered as approximations to stream and isopycnal lines.

III. LEE-WAVE REGIMES FOR A TWO-DIMENSIONAL GAUSSIAN OBSTACLE

In this section we give a brief review of the lee-wave regimes as found for two-dimensional Gaussian obstacles with an aspect ratio, H/L, equal to 0.57. The lee-wave regimes are mainly determined by the Froude number based on H ($F=U/NH$), which quantifies the linearity of the flow, while the Froude number based on L ($F_L=U/NL$) plays a secondary role, quantifying the nonhydrostaticity. Long[1] showed that nonlinear Boussinesq flow over an obstacle can be described by a linear equation (Helmholtz equation) plus nonlinear boundary conditions. We have used Long's model to compute the lee-wave field under the assumption of inviscid flow and an unbounded upper boundary condition. The algorithm used to obtain the solution follows that of Laprise and Peltier,[20] where the governing Helmholtz equation is solved using Fourier transform techniques and where the correct nonlinear lower boundary condition is implemented iteratively. Figures 3(a)–3(d) show the streamlines of the resulting wave fields computed for four different Froude numbers ($F=\{1.2,1,0.97,0.9\}$). The results in Fig. 3(c) show that for $F=0.97$, the streamlines become vertical. This critical Froude number, F_c, thus marks the limit of a statically unstable density gradient where it is generally assumed that

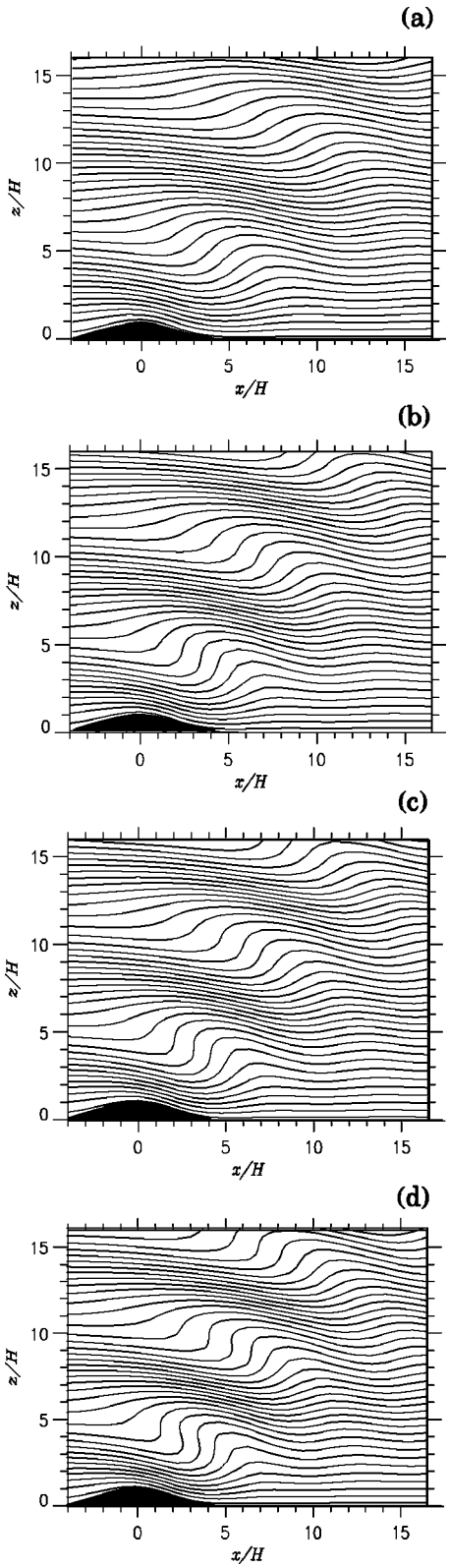

FIG. 3. Streamlines over a Gaussian obstacle ($H/L=0.57$) computed from Long's (1953) two-dimensional inviscid and unbounded model. The flow is from left to right and viewed in the obstacle frame. (a) $F=1.2$, (b) $F=1.0$, (c) $F=0.97$, (d) $F=0.9$.

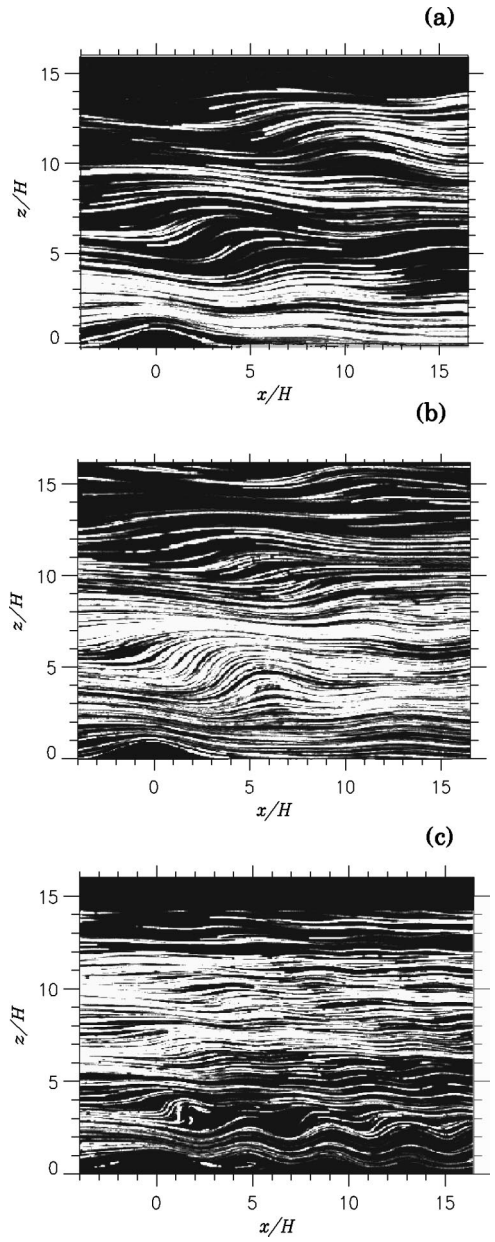

FIG. 4. Pathlines over a two-dimensional Gaussian obstacle ($H/L=0.57$) at Nt=150 and Re=150. (a) $F=1.2$, (b) $F=1.0$, (d) $F=0.6$.

wave breaking is about to occur. Under linear hydrostatic theory (e.g., Queney[21]) vertical steepening occurs for $F_c=1$, but the nonlinear lower boundary condition in addition to the nonhydrostatic effect characterized by F_L yields the slightly lower value of 0.97 for $F_L/F=H/L=0.57$. These nonlinear and nonhydrostatic effects also cause the location of the maximum steepening to move slightly downstream of the obstacle crest.[20,22]

Figures 4(a)–4(c) show experimental wave fields at Nt=150 and Re=150 for $F=\{1.2,1.0,0.6\}$, obtained via particle-streak visualizations. These experimental conditions are viscous and the upper boundary condition is bounded ($D/H=28$) in contrast to Long's model, which is inviscid and unbounded. Nevertheless, for $F=1.2$ [Fig. 4(a)] the wave field can be seen to be in good agreement with Long's solution [Fig. 3(a)] and was also observed to be steady. At $F=1$ [Fig. 4(b)], on the other hand, the flow fluctuated about Long's steady solution over a long time scale (Nt$\sim$50) with occasional breaking. Essentially continuous breaking was observed for $F<0.8$, as shown for $F=0.6$ in Fig. 4(c). The flow can, therefore, be divided into three regimes, a freely propagating wave regime for $F>1$, an intermittent wave-breaking regime for $1>F>0.8$, and a lee-wave breaking regime for $F<0.8$. The remainder of this paper, focusing on the breaking regime, will be undertaken at $F=0.6$.

IV. LEE-WAVE BREAKING PROCESS

A. Overview of transient evolution

Since the flow starts impulsively from rest, we begin by examining the transient evolution leading to wave breaking. Using a two-dimensional obstacle in the small tank (Re=150), the flow was simultaneously examined in two orthogonal planes in order to gain an understanding of possible three-dimensional aspects. The two planes chosen were the vertical (xz) symmetry plane ($y/H=0$) and the horizontal (xy) plane through the center of the wave breaking region ($z/H=3$). In the vertical plane, the flow was visualized using particle-tracking in order to identify the wave field. In the horizontal plane, fluorescent dye visualization with fixed vertical sheets was used in order to verify the two-dimensionality of the flow. Figures 5(a)[i–vii] and 5(b)[i–vii] show the results at various stages of evolution leading to wave breaking (Nt=$\{20,24,34,38,42,46,51\}$). Figures 5(a)[i–vii] show the pathlines in the vertical (xz) plane while Figs. 5(b) [i–vii] show the simultaneously obtained dye or streaklines in the horizontal (xy) plane. Although the vertical sheets of dye were introduced into the fluid just prior to the tow and were initially parallel and straight, weak large-scale horizontal background motions which generate deformations by the time of the tow are usually unavoidable. Fortunately, however, these deformations can be distinguished from the smaller-scale deformations induced by the flow when viewing the continuous evolution recorded on video. Thus, the main features that can be interpreted from the visualizations in Fig. 5, in conjunction with the video, are depicted in Fig. 6, for clarity.

In Figs. 5(a–i) and 6(a–i), at Nt=20, it can be seen that the wave on the lee-side of the obstacle is still steepening. By Nt=24 [Figs. 5(a-ii) and 6(a-ii)] the wave is vertical and has, therefore, reached the critical condition where the local flow becomes unstable. However, this condition is only statically unstable. Rather than evolving directly and rapidly into a ''turbulent'' zone, the wave slowly overturns into the form of an ''S,'' as seen in Figs. 5(a-iii) and 6(a-iii) at Nt=34. Fourteen buoyancy periods after reaching the critical condition, at Nt=38, the flow is still overturning with the maximum unstable inclination of the wave approaching about 55° with respect to the vertical [Figs. 5(a-iv) and 6(a-iv)]. Similar observations of S-shaped isopycnals which persist for long periods compared to the wave period were also made by Thorpe[23] in the case of a stratified fluid oscillating in a rectangular tube. In agreement with the present results, Thorpe concluded that the selection of a condition in which isopyc-

nals become vertical as a limit for finite amplitude evolution of internal waves may be arbitrary and unrealistic.

Figures 5(b)[i–iv] and 6(b)[i–iv] show the corresponding horizontal plane results. They reveal that the flow remains essentially two-dimensional up to Nt=38, even though the wave has overturned. The only spanwise motions that can be inferred are large-scale deformations which are due to the background disturbances in the tank. Repetitions of the experiment confirmed that these deformations are uncorrelated with the dynamics of the wave breaking process.

In the late stages of the overturning, the S-shape does not remain symmetric: At Nt=38 [Figs. 5(a-iv) and 6(a-iv)],

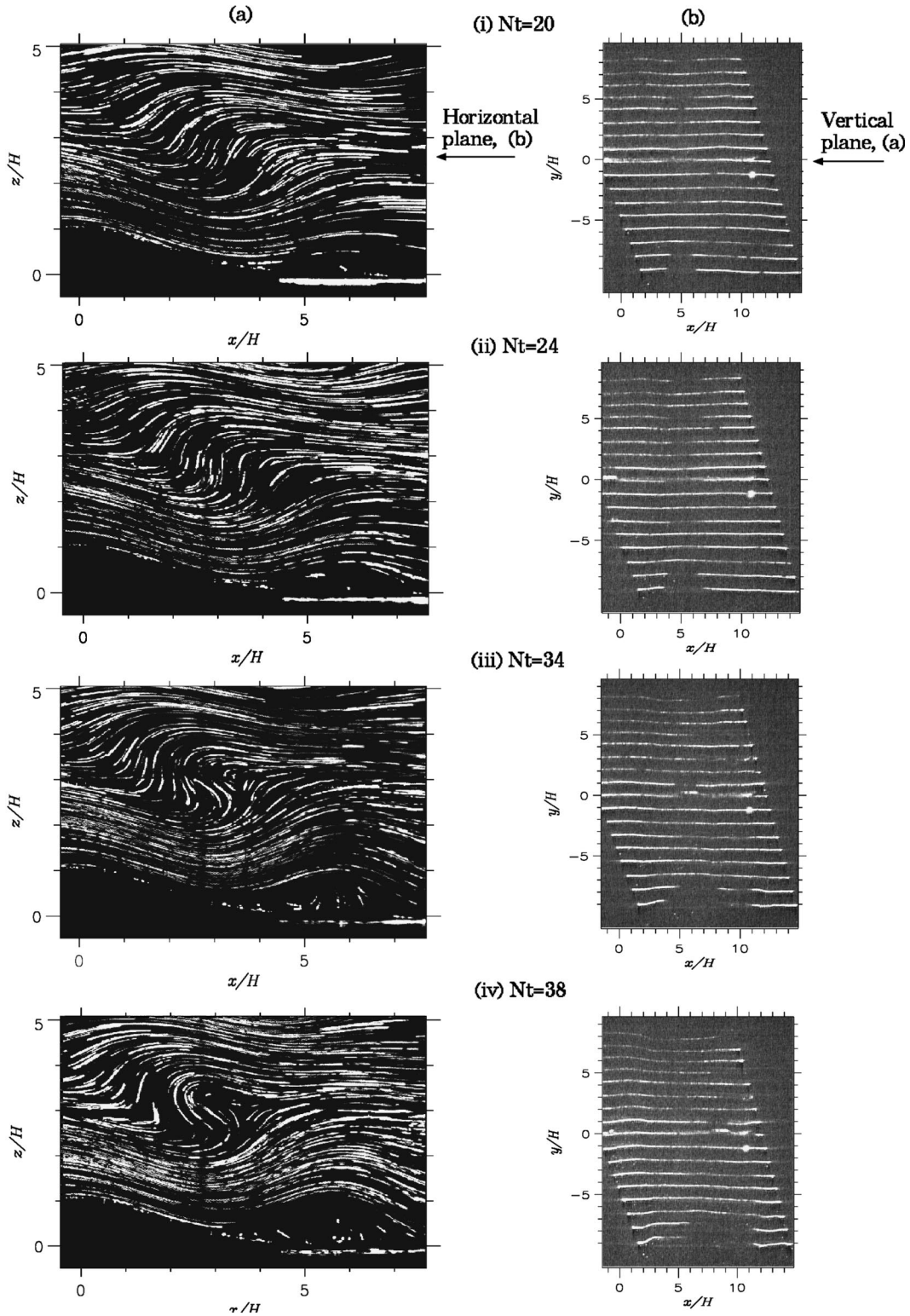

FIG. 5. Simultaneous flow visualizations in two planes intersecting the wave breaking region over a two-dimensional Gaussian obstacle (Re=150) at Nt={20,24,34,38,42,46,50}. (a) Pathlines in vertical (xz) plane at $y/H=0$, (b) fluorescent-dye images in horizontal (xy) plane at $z/H=3$.

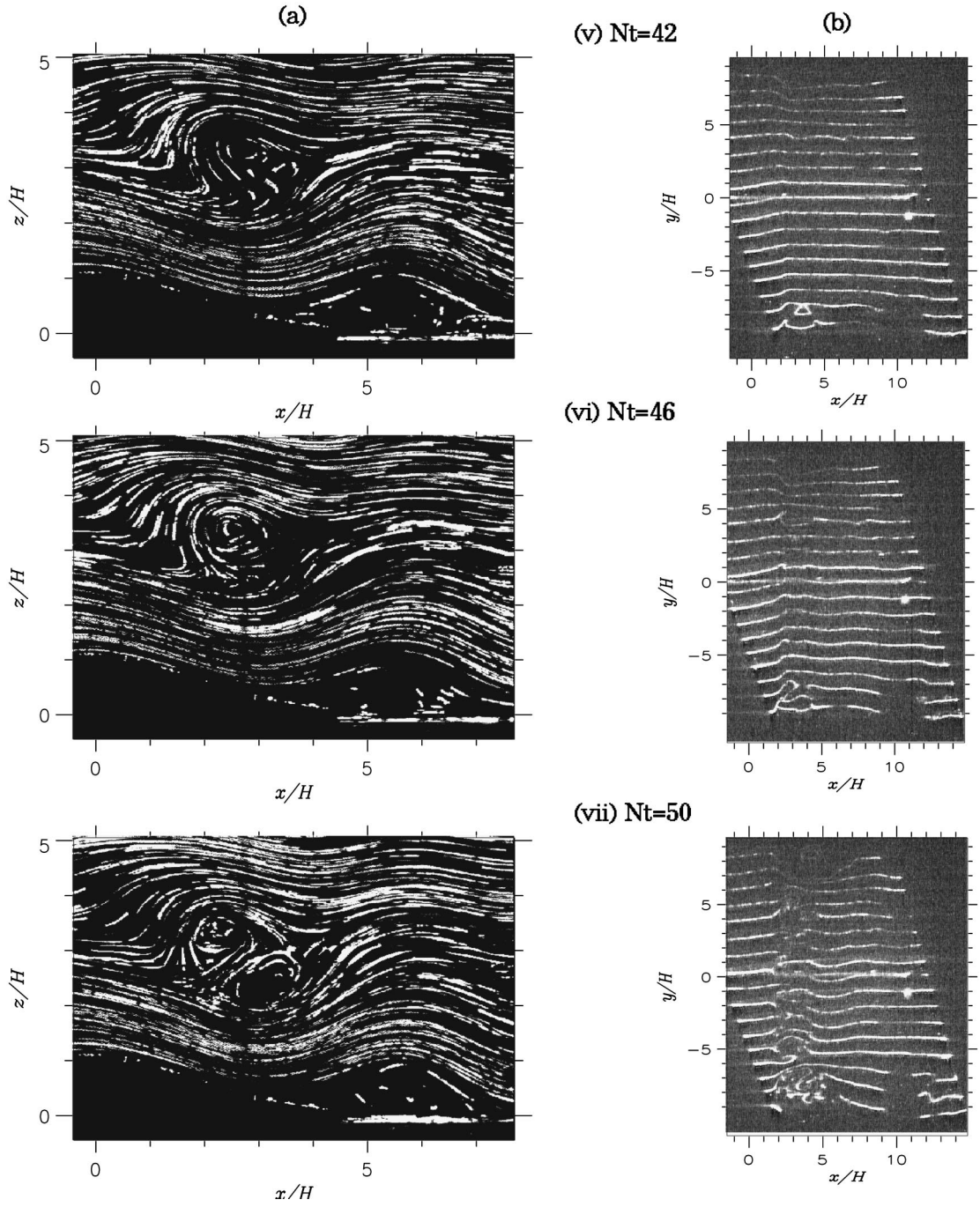

FIG. 5. (*Continued.*)

it can be seen that the upper half of the S has contracted more than the lower half. A few buoyancy periods later, at Nt=42, this contraction of the upper half of the overturning wave leads to a topological change in the structure of the flow: The formation of a clockwise rotating vortex [Figs. 5(a-v) and 6(a-v)]. The emergence of this vortex is directly associated with the appearance of a saddle point downstream, as it must in order to satisfy the kinematic demands of the flow. Interestingly, except near the walls of the tank, the flow has essentially remained two-dimensional in the breaking zone during this process since no significant spanwise motions can be detected in the horizontal plane [Figs. 5(b-v) and 6(b-v)]. The implication is that a quasi two-dimensional spanwise (ω_y) vortex has developed. However, significant spanwise motions can be observed near the edges of the flow, suggesting that the billow does not remain two-dimensional over the entire width of the obstacle.

The vortex continues to grow for several buoyancy periods as seen in the vertical (xz) plane results at Nt=46 [Fig. 5(a-vi)]. At this stage, however, significant spanwise motions can be inferred from the kinks apparent in the streaklines, suggesting that the motion has become three-dimensional. A few buoyancy periods later, by Nt=50, the topology of the flow has again undergone a topological change [Figs. 5(a-vii)

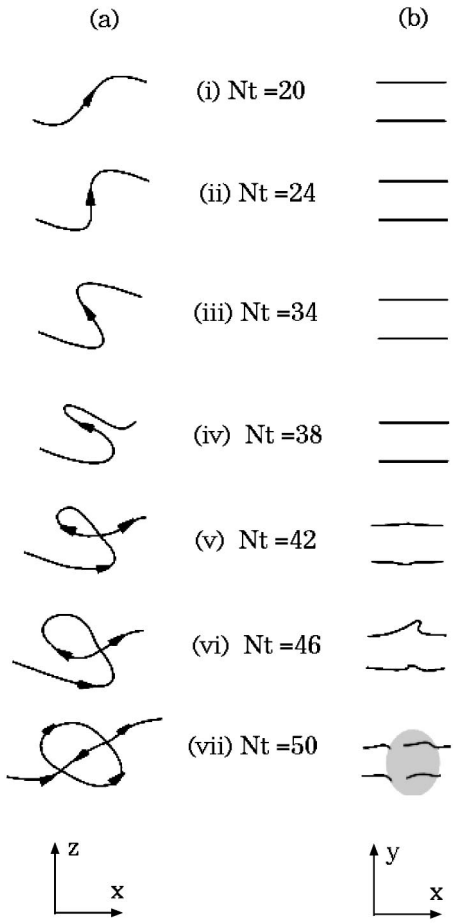

FIG. 6. Corresponding schematic representation of the flow visualizations results shown in Fig. 5. (a) Vertical (xz) plane, (b) horizontal (xy) plane.

and 6(a-vii)]. The flow now consists of two counter-rotating vortices in conjunction with two (necessary) saddle points. In the horizontal (xy) plane [Figs. 5(b-vii) and 6(b-vii)], the streaklines have become very perturbed in the spanwise direction, i.e., implying that the flow has become highly three-dimensional.

B. Primary instability

The preceding results show that the first wave breakdown yields a spanwise (ω_y) vortex. This is essentially a two-dimensional process since no significant spanwise motions over the central portion of the obstacle crest were detected. The two-dimensionality is confirmed by the consistent observations of spanwise vortices forming in the fixed $y/H=0$ vertical plane for all repetitions of the experiment. The ensuing counter-rotating vortex pair, on the other hand, was not consistently observed. Since three-dimensional structures are expected to yield different topologies depending on their position relative to a fixed plane of visualization while a two-dimensional structure necessarily yields the same topology, the consistent observations of spanwise vortices support the conclusion that the single spanwise vortex formation is essentially two-dimensional, whereas the ensuing vortex pair formation is three-dimensional as suggested in Figs. 5(b-vii) and 6(b-vii), and demonstrated in Sec. IV C.

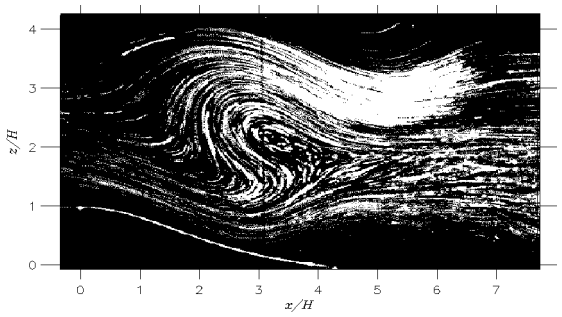

FIG. 7. Pathlines in the vertical center plane over a quasi two-dimensional obstacle in the large tank. The obstacle measures 1.14 m (length) by 2.5 m (width) by 0.13 m (height). Re=8000, Nt=21.

The emergence of a spanwise vortex in the fixed $y/H=0$ vertical plane after the wave overturns into an S-shape was also observed with the quasi two-dimensional Gaussian obstacles for all Reynolds number magnitudes investigated, including the high Reynolds number magnitude under fully turbulent conditions (Re$\sim 10^4$). It can, therefore, be considered that the uniform extent of the quasi two-dimensional obstacle is wide enough such that the overturning wave breaks down as with the two-dimensional obstacle. In addition, this breakdown appears to be independent of the Reynolds number. Figure 7 displays the pathlines in the central vertical plane at Re=8000 for a quasi two-dimensional obstacle. Clearly, as in the lower Reynolds number experiments, a clockwise vortex can be identified after the wave has overturned into an S-shape.

Details of the flow conditions just prior to the spanwise vortex roll-up have been investigated by applying the PIV technique to the particle visualizations of the Re$\sim$600 experiments. Assuming streamlines to be approximately equal to isopycnals for this slowly evolving flow, vertical density profiles [$\rho(z)$] could also be estimated by evaluating the value of each isopycnal at the upstream density gradient. Figure 8 shows a PIV velocity vector field in the $y/H=0$ vertical plane just prior to the clockwise vortex formation. The flow was generated by towing a quasi two-dimensional

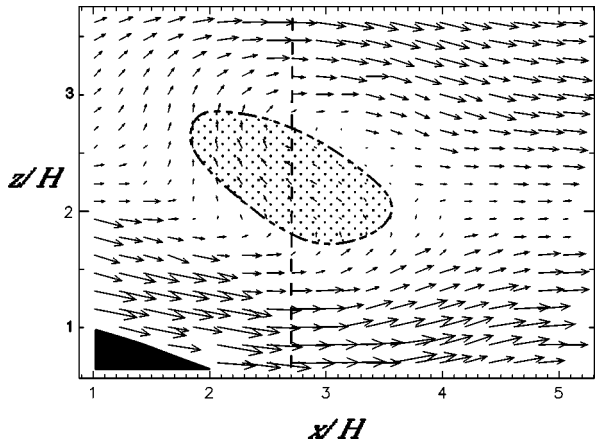

FIG. 8. Velocity vector field in vertical (xz) plane at $y/H=0$ obtained via PIV. Re=580, Nt=24, quasi-two dimensional obstacle. The shaded region is statically unstable. (The dashed line shows the position of the profiles presented in Fig. 9.)

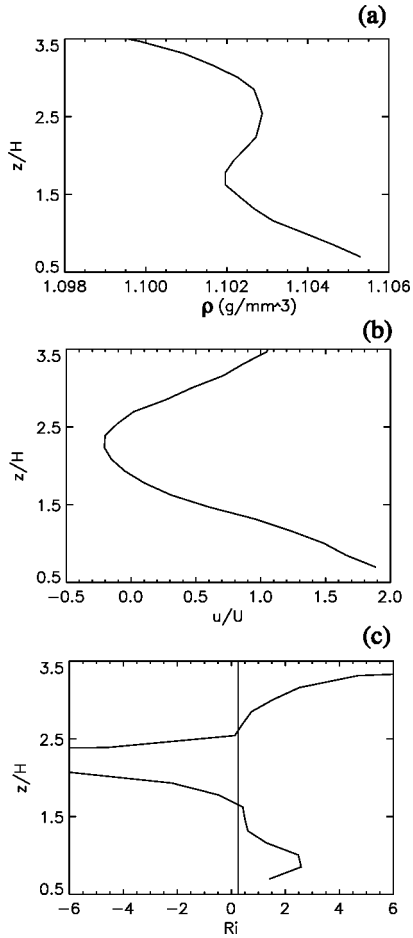

FIG. 9. Vertical z profiles at $x/H=2.7$ for Re=580, Nt=24, quasi two-dimensional obstacle. The location of the profiles is indicated by the dashed line in Fig. 8. (a) $\rho(z)$, (b) $u(z)/U$, (c) Ri(z).

obstacle. It can be seen that the velocity vector field corresponds closely to the pathline field depicted in Fig. 5 for the case of the two-dimensional obstacle at lower Reynolds number just prior to the vortex roll-up, specifically a S-shape with the top portion of the S being more contracted than the bottom. The cross-hatched zone in Fig. 8 identifies the region where the streamlines and thus the isopycnal lines have overturned, rendering this region of the flow statically unstable.

Figures 9(a)–9(c) show the corresponding density, velocity and gradient Richardson profiles [$\rho(z)$, $u(z)$, and $Ri(z)=N^2/(du/dz)^2$] through the center of the overturned wave at $x/H=2.7$. Similar to the vertical phase-relationship between the shear and stratification profiles analyzed by Winters and Riley,[24] it can be seen that regions of strong shear coincide with stable stratification and regions of weak shear with unstable stratification. Near the boundaries of the statically unstable fluid, the shear is strongest and $Ri(z)$ lies between 0 and 0.25 for a thin region outside the boundaries of the statically unstable region. Thus, shear instability can occur according to the theorem of Miles[25] and Howard[26] since $0<Ri<0.25$ somewhere in the flow. Of course, this criterion is strictly only valid for parallel and horizontal shear as well as infinite Re number, and the condition for convective instability is simultaneously satisfied since $Ri<0$ below.

The stability analysis of Winters and Riley,[24] examining internal wave-breaking near a critical layer, showed that the type of instability, shear or convective, which generates the fastest growing mode with spanwise vortices depends on the relative importance of the unstable stratification with respect to the shear. Using perturbations in the xz-plane they found that streamwise convective instability (i.e., convective instability resulting in spanwise vortices) becomes only dominant for vanishing shear. Strong shear, on the other hand, completely inhibits streamwise convective instability; instead the spanwise vortices grow due to the kinetic energy of the shear. At intermediate shear values, the instability of the fastest growing mode is due to both shear and convective effects and is similar in appearance as in the strong shear situation. Winters and Riley[24] show that the relative importance of shear with respect to unstable stratification for the fastest growing modes is determined by the bulk Richardson number, $J=(NL_c/U_c)^2$, where U_c and L_c are characteristic scales of the shear profile. For the ''strong'' shear situation J never exceeds 0.25. ''Intermediate'' shear values are for values of J just above 0.25 while ''vanishing'' shear occurs in the large J limit. In the present flow, where a similar phase-relationship between the unstable density profile and the shear profile occurs prior to the formation of a spanwise vortex, J was estimated to be about 0.18 from the density and velocity profiles shown in Figs. 9(a) and 9(b). (U_c was correspondingly taken as the velocity defect and L_c the width of the defect.) The value of J being smaller than 0.25 suggests that shear is the main driving force with the convective contribution playing a minor role in the formation of the spanwise vortex.

Using disturbances in the yz-plane which are not influenced by the shear in the xz-plane, Winters and Riley[24] show that for the fastest growing modes, spanwise convective instability, yielding modes with streamwise vortices, exists for $J<0.25$. Linear stability theory predicts that this streamwise mode grows at about half the rate as the spanwise mode, from which they conclude that the instability is three-dimensional. Rather than being truly three-dimensional, we observed that the spanwise vortex in a given xz-plane is associated with a quasi two-dimensional vortex extending along the y direction. Small streamwise deformations associated with this vortex could be the result of streamwise convective instability, but do not appear significant in the experiments, as would be expected from their smaller growth rate compared to that of the shear instability generating the spanwise vortex.

C. Secondary instability

The simultaneous views of the vertical and horizontal planes discussed in Sec. IV A showed that shortly after the spanwise vortex has formed, the lower portion of the S-shaped wave (in the vertical plane) forms into a vortex of opposite rotation (at Nt=50), thus yielding a counter-rotating vortex pair. Simultaneously, in the horizontal plane, the previously unperturbed and uniform flow becomes

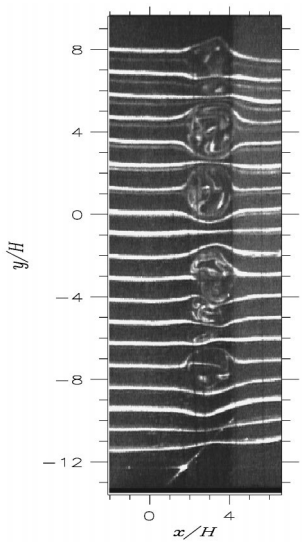

FIG. 10. Fluorescent-dye image in horizontal (xy) plane at $z/H=2.5$. Re=150, Nt=50, quasi two-dimensional obstacle.

strongly perturbed, implying that this evolution is three-dimensional in nature. A more detailed fluorescent dye visualization in the horizontal plane at the level of breaking, also performed with a quasi two-dimensional obstacle at Re=150, is shown in Fig. 10 for Nt=50. It clearly shows thatseveral separate structures in the xy-plane have formed at the same time as the spanwise counter-rotating vortex pair. For example, near the center of the picture, an undeformed streakline can be seen between two adjacent structures. Clearly, the initially quasi two-dimensional spanwise vortex has separated into distinct structures.

Figure 11 shows the pathline pattern at the same time as above (i.e., Nt=50), but in the frontal (yz') plane intersecting the wave-breaking region. This plane is slightly inclined at 13° with respect to the z axis (defined as z') so that the flow can be viewed through the surface of the water. Two parallel cameras were used in order to span a wider extent of the flow and the laser-light sheet was made relatively thick (~1 cm) to capture the vortex motion. Outside the wave-breaking region the pathlines are expected to be vertical and their apparent inclination in Fig. 11 which increases towards the edges in each view is due to the movement of the particles through the laser sheet. Nevertheless, the pathlines in the wave-breaking region reveal counter-rotating circulatory patterns indicating the presence of counter-rotating streamwise vortices, characteristic of streamwise convective instability as observed (numerically) by Winters and Riley[24] and also by Andreassen *et al.*[13] or Afanasyev and Peltier.[9]

Afanasyev and Peltier,[9] who present a three-dimensional numerical simulation of stratified flow over topography, propose on the basis of their numerical simulations as well as the preceding laboratory experiments of Voropayev *et al.*[27] in an overturned linearly stratified fluid, that thin pairs of horizontal layers of relatively lighter and denser fluid form as a result of the vertical isopycnals of the steepening wave. These layers subsequently become unstable, resulting in the formation of arrays of mushroom-like convective structures in the yz-plane. They conclude that the streamwise vortices are created by the shear-aligned convective instability mechanism of Klassen and Peltier.[10]

In the present laboratory experiments, the unstable system does not consist of several pairs of unstable layers but instead of a heavy spanwise vortex lying above a light layer of unstable fluid. Yet, similar to the convective mushroom-like structures observed by Voropayev *et al.*[27] or Afanasyev and Peltier,[9] this system is subsequently observed to become unstable with significant up and down-drafts associated with streamwise convective structures (Fig. 11). However, the occurrence of a second spanwise (counter-clockwise) vortex which has been observed to form simultaneously is, given the results in the other planes, necessarily part of a three-dimensional structure. Similar spanwise vortices were not reported in the studies by Afanasyev and Peltier[9] and Voropayev *et al.*[27] Thus, there appear to be differences between the observed mechanisms.

In the topographic flow simulations of Afanasyev and Peltier[9] these differences are likely due to their use of a free-slip boundary condition. Recent direct numerical simulations at Re=200 by Gheusi *et al.*[28] of the same flow as discussed here over a two-dimensional obstacle have shown that a free-slip condition on the surface of the obstacle results in a mixed layer which continuously extends downstream (rather than being confined above the lee-slope), and both the

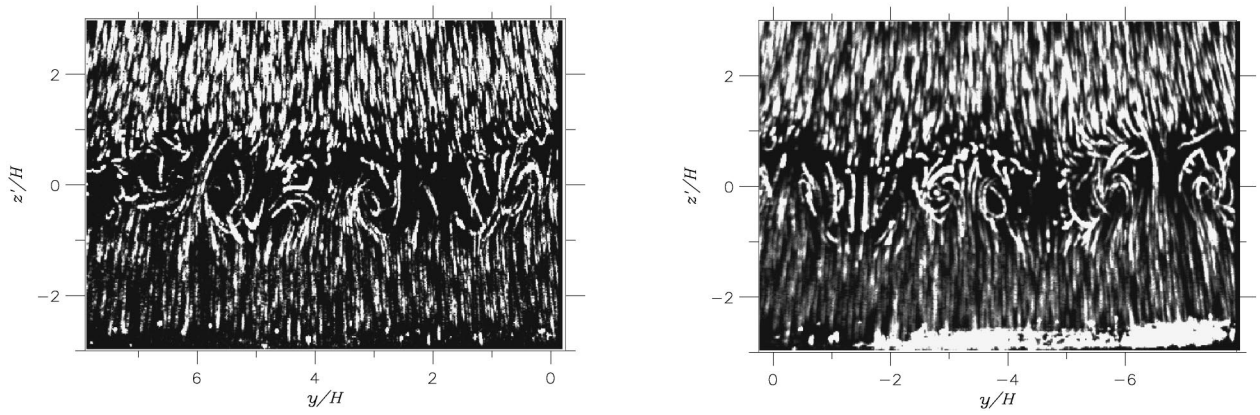

FIG. 11. Pathlines in the frontal (yz') plane through the wave-breaking region. Re=150, Nt=50, quasi two-dimensional obstacle.

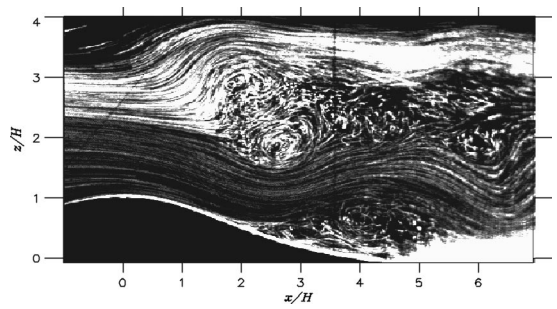

FIG. 12. Pathlines in the vertical $y/H=0$ plane at high Reynolds number over a quasi two-dimensional obstacle. Re=8000, Nt=118.

mixed layer and the associated lower layer of accelerated fluid propagate downstream. Furthermore, no trapped lee-wave is observed anymore and the maximum downslope wind speed has accelerated to about $3.5U$, higher than the situation when surface friction is accounted for ($\sim 2.3U$, in agreement with the experiments). Similar observations were also made by Richard *et al.*[29] In the topographic flow simulation with a free-slip condition of Afanasyev and Peltier,[9] a similar propagative character was observed. Thus, the streamwise confinement is effectively removed, yielding a convective instability with predominantly streamwise vortices. In the case of the experiments by Voropayev *et al.*,[27] the overturned tank is very narrow in the streamwise direction, which could inhibit spanwise structures by being narrower than the wavelength of this amplified disturbance.

V. DOMINANT VORTEX STRUCTURES

A. Vortex model

The emergence of the second spanwise vortex yields a counter-rotating vortex pair as seen in Fig. 13(a-i) at low Reynolds number (150) or in Fig. 12 at high Reynolds number (8000). The streamline pattern of these counter-rotating vortex structures is represented in Fig. 13(a-ii). However, this topology, which is independent of the Reynolds number, does not always occur in the vertical planes after the three-dimensionalization. Instead, a different topology can sometimes be identified as seen in Fig. 13(b-i) and in the corresponding streamline pattern in Fig. 13(b-ii). A common feature that was observed in these cases is that the critical points (focal and saddle points) have disappeared and that the flow in the wave-breaking region is upward and streamwise. Usually one or both of the negative and positive open bifurcation lines seen in Fig. 13(b-ii) can be identified, which indicates that the flow is not two-dimensional since the divergence is nonzero.

In the frontal (yz') plane through the wave-breaking region (Fig. 11), several pairs of adjacent counter-rotating vortex pairs were identified, while in the horizontal (xy)

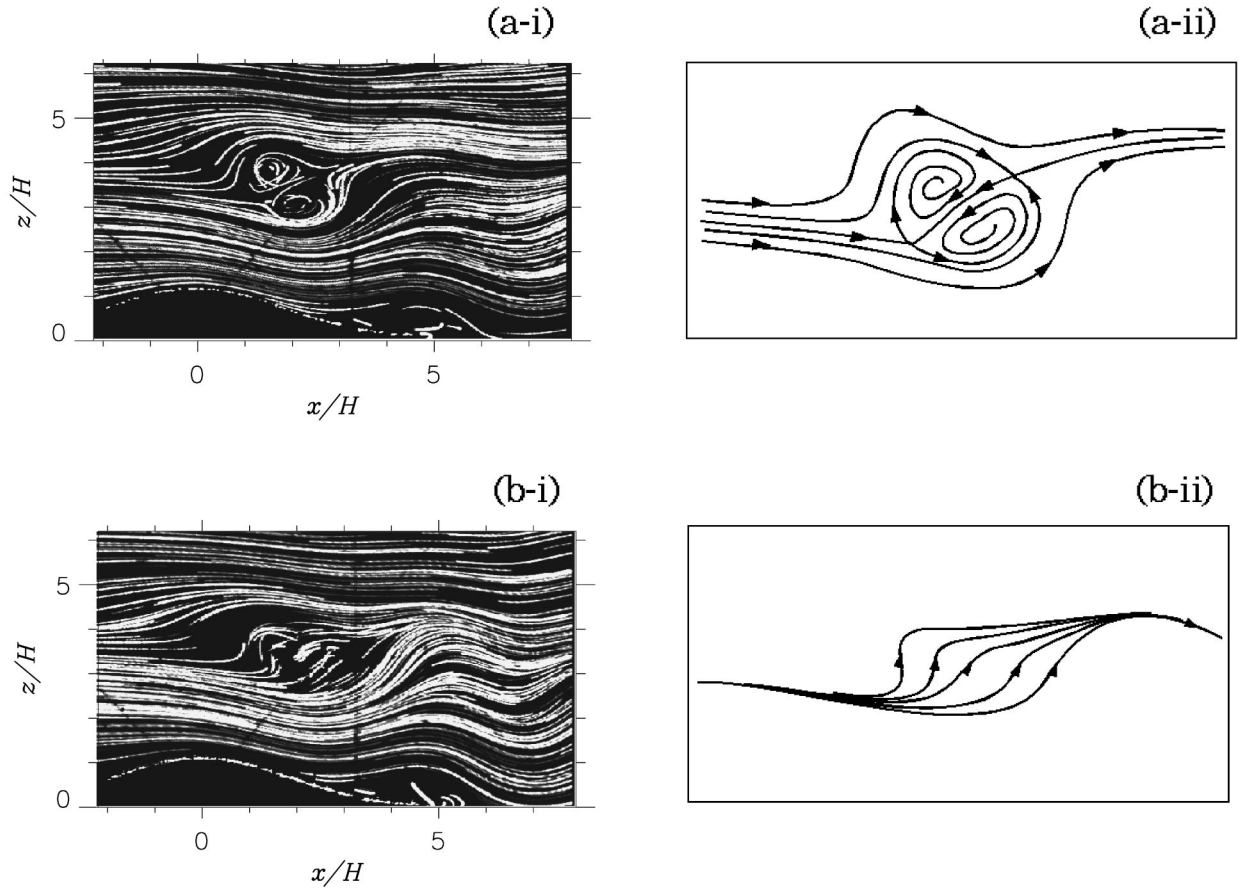

FIG. 13. Sectional streamlines deduced from particle-tracking results in the $y/H=0$ vertical (xz) plane (Re=150). Two different topological patterns can be observed: (a) Two counter-rotating focal points with two saddle points, and (b) no focal nor saddle points.

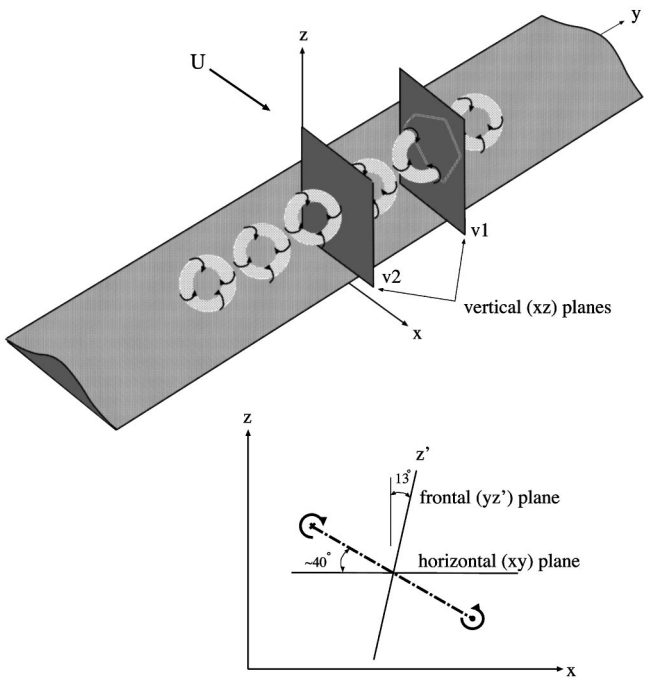

FIG. 14. Proposed vortex skeleton model of the dominant structures in the wave-breaking region over an obstacle. The co-rotating toroidal structures are inclined and, therefore, exhibit strong vorticity components in all three directions. The three planes of investigation are indicated with respect to the inclined vortices.

plane, the fluorescent dye visualizations (Fig. 10) have revealed distinct structures. To account for these topological features in the three planes, the vortex model shown in Fig. 14 is proposed. The vortex structures are toroidal or ring-like and are inclined with respect to the horizontal. In this configuration they are associated with strong vorticity components in all directions. Sectional streamlines in a vertical plane intersecting the flow near the center of a torus (plane v1 in Fig. 14) would reveal the topology of Fig. 13(a). On the other hand, no foci but strong upward flow as in Fig. 13(b) would be observed in a vertical plane positioned in the region between two adjacent tori (plane v2 in Fig. 14). Bifurcation lines are expected since in a real flow a perfect symmetry plane is unlikely to exist and furthermore unlikely to be coplanar with the plane of examination. Since in the experiment the vertical plane of examination was fixed with respect to the obstacle, the observed changes of topology between the ones depicted in Figs. 13(a) and 13(b) would be the result of spanwise advection of the vortices. While sectional streamlines in a vertical plane through the center of a torus yield one counter-rotating vortex pair, sectional streamlines in frontal (yz') and horizontal (xy) planes through the array of vortices are expected to yield several aligned counter-rotating vortex pairs (Fig. 15), each pair associated with one torus.

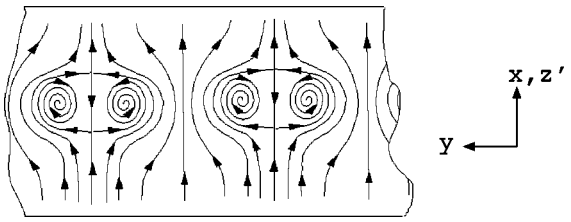

FIG. 15. Sectional streamline pattern deduced from the vortex model in either the horizontal (xy) or frontal (yz') planes. The planes intersect the centers of the vortices.

B. Experimental confirmation

Simultaneous measurements in at least two planes are needed to confirm that the observed topologies in each plane can indeed be attributed to the type of three-dimensional vortex structures proposed in the model. Similar simultaneous fluorescent-dye and particle tracking experiments as described in Sec. IV A were carried out at Re$\sim$150 for both the two-dimensional and the quasi two-dimensional obstacles. They revealed that the ''relaminarized'' topology of Fig. 13(b) exists between two adjacent structures in the horizontal plane while the counter-rotating vortex pair is observed between adjacent structures [Fig. 13(a)]. The fluorescent dye in the horizontal plane, however, did not clearly reveal the topology of those structures and therefore experiments examining the vertical and horizontal planes simultaneously with the particle tracking technique were carried out at Re$\sim$600 for both types of obstacles.

The results for the quasi two-dimensional obstacle with the xz-plane fixed at $y/H=0$ and the xy-plane at $z/H=2.5$ are shown in Figs. 16(a)[i–ii] and 16(b)[i–ii], respectively. The horizontal (xy) plane at Nt=64 shown in Fig. 16(b-i) reveals at least two counter-rotating vortex pairs in the wave-breaking region, roughly aligned along the spanwise direction. Taking into consideration the senses of rotation of these structures, it can be inferred that two pairs are centered around $y/H\sim 0$. Therefore, no critical points are expected in the $y/H=0$ vertical plane, which is verified by the inferred sectional streamlines in Fig. 16(a-i). At Nt=128, one vortex pair can be identified in the horizontal plane [Fig. 16(b-ii)]. Since the center of the vortex pair is now aligned laterally around $y/H\sim 0$, we expect a counter-rotating vortex pair to appear in the $y/H=0$ vertical plane—as evident in the results displayed in Fig. 16(a-ii). Thus, these experiments confirm the three-dimensional topological features expected from the presence of toroidal vortices.

C. Spanwise alignment and scales

According to the proposed vortex model, the topology in either the horizontal (xy) or the frontal (yz') planes consists of a spanwise array of counter-rotating vortex structures as depicted in Fig. 15. This topology is in agreement with the one inferred from the pathline patterns in the frontal plane shown previously in Fig. 11 for a two-dimensional obstacle at Re=150. Pathline patterns in the horizontal plane, for the same obstacle and Reynolds number magnitude, are shown in Figs. 17(a) and 17(b). In this plane two cameras were overlapped with separate zooms. The narrow zoom in Fig. 17(b) clearly shows two counter-rotating vortex pairs aligned in the spanwise direction. The wide zoom in Fig. 17(a) re-

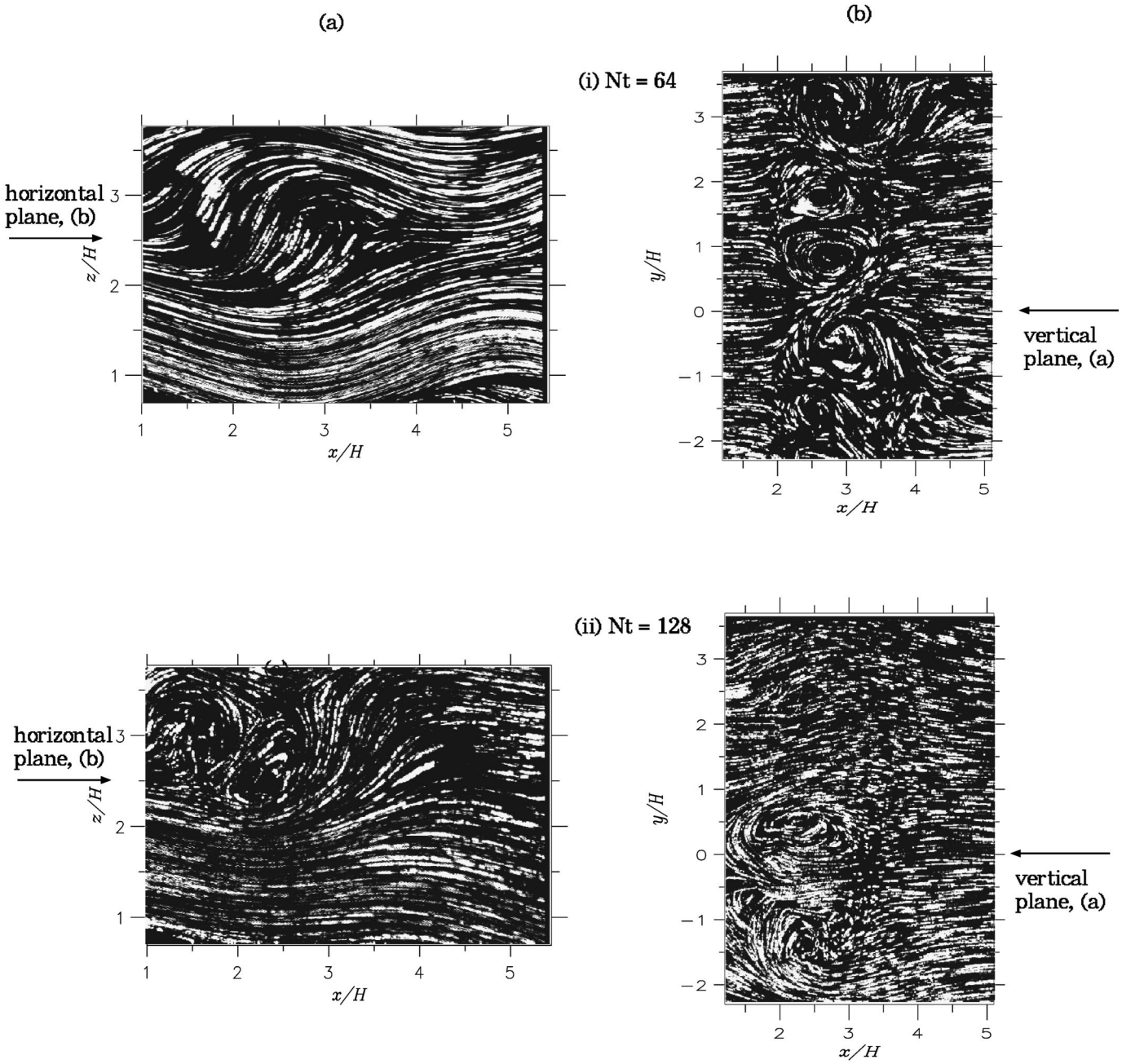

FIG. 16. Simultaneous particle-tracking results in the vertical (xz) plane at $y/H=0$ and the horizontal (xy) plane at $z/H=2.5$, intersecting the wave breaking region. Re=580, quasi two-dimensional obstacle. (a) xz-plane: (i) Nt=64, (ii) Nt=128; (b) xy-plane: (i) Nt=64, (ii) Nt=128.

veals one additional pair and possibly two more. Assuming symmetry of the flow, about six vortex pairs are, therefore, aligned parallel to the obstacle crest, spanning about half the obstacle width. Outside of this region, three-dimensional effects due to the presence of the walls are evident.

The spanwise separation between the centers of the vortex pairs apparent in Fig. 17 ranges from about 1–1.5 H. Given that six pairs span about 16 H, the average center-to-center spacing is found to be about 1.3 H, implying that one pair extends over 2.6 H. In the other planes of the flow, roughly the same scales were observed (cf., Figs. 11 and 5), suggesting that the structures are approximately ring-like as depicted in Fig. 14. For the quasi two-dimensional obstacle at Re=580 shown in Figs. 16(a-ii) and 16(b-ii), the vortex spacing, although slightly larger in this instance, is about 2 H in both the simultaneously sampled vertical and horizontal planes, suggesting that the ring-like nature is independent of this Reynolds number range as well as the obstacle shape. The average wavelength of the vortex spacing for the quasi two-dimensional obstacles at both Reynolds numbers examined also appears to be independent of these two factors, ranging from about 1 to 2H, while up to three pairs could be identified over the uniform section of the obstacle crest. It can be noted that the numerical simulations at Re=200 over a two-dimensional obstacle by Gheusi *et al.*[28] revealed characteristic lateral (y) wavelengths of about 2.4–4 H independently of the different types of initial perturbations applied (white noise, harmonic or lateral walls). These wavelengths

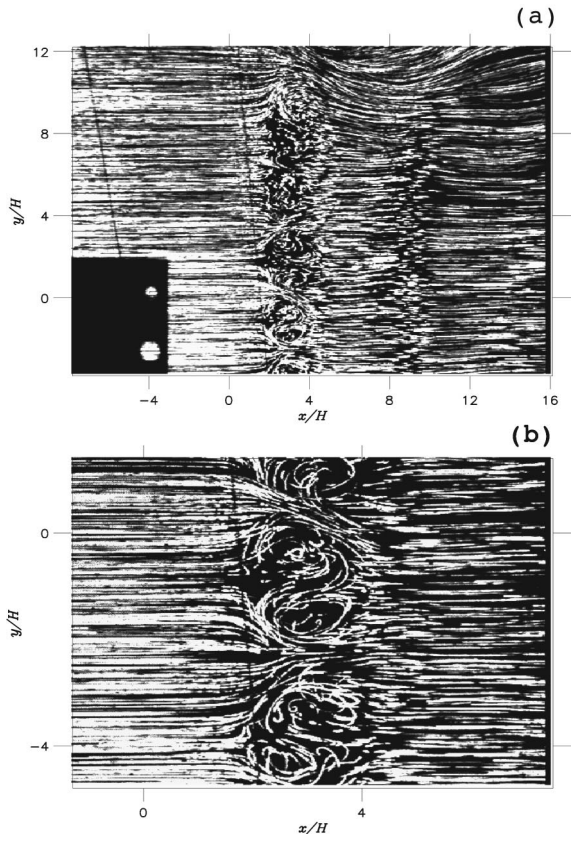

FIG. 17. Pathlines in the horizontal (xy) plane at $z/H=2.5$. Re=150, Nt=50, quasi two-dimensional obstacle. (a) Wide zoom with camera one; (b) Narrow zoom with camera two.

also correspond to a vortex spacing of 1.2–2 H, in agreement with the range of experimental values.

VI. CONCLUSION

Experiments were carried out to characterize the lee-wave breaking process and the resulting large-scale structures. The experiments with two dimensional Gaussian-shaped obstacles covered the low Reynolds number magnitudes 10^2 and 10^3 and those with quasi two-dimensional Gaussian-shaped obstacles also covered the turbulent Reynolds number magnitude 10^4. Independent of those Reynolds numbers or obstacle shapes, the results have shown that the initial wave steepening as well as the subsequent wave overturning into a S-shape are two-dimensional. As a result of this two-dimensional overturning a single roller parallel to the obstacle crest forms. This spanwise roller extends over a significant portion of the uniform section of either the two dimensional or the quasi two-dimensional obstacle. Subsequently, the flow in this region becomes highly three-dimensional, leading to counter-rotating vortex pairs in all three planes of the flow.

A vortex model is proposed to account for the dominant large-scale counter-rotating vortex pairs. It consists of toroidal or ring-like vortices aligned in the spanwise direction, the planes of which are inclined with respect to the horizontal ($\sim 40°$). The center-to-center vortex spacing of these rings in all directions is about 1 to 2 H, roughly the height of the overturning region, and was found to be independent of the Reynolds numbers or the obstacle shapes examined. In the case of the two-dimensional obstacle about six rings have been identified, spanning roughly half the total obstacle width, beyond which the flow is three dimensional due to the wall effects. For the quasi two-dimensional obstacle, up to three rings have been identified, spanning almost the extent of the uniform section of the obstacle ridge.

The presence of separate ring-like structures explains the initially perplexing results in the vertical planes. The streamlines in these planes were occasionally marked by the absence of critical points in the wave-breaking zone, similar to the wave steepening but occurring after a period of strong wave-breaking activity. Such an apparent relaminarization in the wave breaking region could be interpreted as a decay of the wave-breaking activity, if three-dimensional effects are not considered. However, rather than being relaminarized, the strong wave-breaking activity is concentrated in separate zones whose large-scale organization takes the form of ring vortices. Adjacent to such vortices, on the other hand, the flow is relatively calm with no critical points. Spanwise advection of the vortex structures will cause a shift in the flow patterns observed in any fixed vertical plane and explain the apparent relaminarization.

The primary instability takes the form of a quasi two-dimensional spanwise vortex. In analogy with similar shear and stratification profiles as those analyzed by Winters and Riley,[24] the bulk Richardson number computed from the unstable stratification and shear profiles just prior to the vortex formation suggests that this instability is essentially shear driven since the contribution of convective instability in the vertical (xz) plane is small. Winters and Riley[24] predict that convective instability in the yz-plane has a smaller growth rate than the shear instability in the xz-plane which is consistent with our observation of a quasi two-dimensional spanwise vortex without the appearance of significant streamwise vortices. The results are also in agreement with Deardorff[30] who showed that the critical Rayleigh number in the presence of shear is higher for spanwise than for streamwise structures, implying that shear will inhibit streamwise convective instability (yielding spanwise rolls), but not spanwise convective instability (yielding streamwise rolls).

The ensuing secondary instability is highly three-dimensional and displays some of the features of the shear-aligned convective instability mechanism observed by Afanasyev and Peltier[9] in that a strong mode with streamwise vortices is observed. These streamwise vortices, however, are not in the shape of long streamwise rolls, but are instead part of the inclined ring-vortices with significant components of vorticity in all directions. Each ring vortex is associated with a strong central down-draft, so that the structures closely resemble those resulting from a three-dimensional Rayleigh–Taylor instability as shown numerically by Tryggvason and Unverdi.[31] These authors examined the fully three-dimensional deformation of an interface between two fluids in the limit of weak stratification in a rectangular domain perturbed by a two-dimensional disturbance and found that as a ''blob'' of heavy fluid falls down, the baroclinically generated vorticity forms a closed vortex ring around this

blob. Jacobs and Catton[32] who examined the case of a large density difference concluded that disturbances more or less equally proportioned in the lateral directions were favored, which would also be in agreement with the formation of ring-vortices.

The present work has examined the large-scale dynamics of lee-wave breaking and also provided the basis for the low Reynolds number direct numerical simulations using a non-hydrostatic atmospheric model (Meso-NH).[28] The next aim is to study the turbulence characteristics of the wave-breaking region via velocity and density measurements in the wave-breaking region in the large tank at $\mathrm{Re}\sim 10^4$. This will allow further validation of the numerical model, in particular the sub-grid turbulence closures for high Re conditions. The validated model can then be used to study atmospheric conditions with $\mathrm{Re}=\infty$.

ACKNOWLEDGMENTS

This work was financially supported by Météo-France, a TMR Marie Curie Research Training Grant (O. Eiff) and the CNRS program PATOM. We are also very grateful to each member of the Simulation Physique des Ecoulements Atmosphériques team from the Centre National de Recherches Météorologiques at Météo-France for their help.

[1] R. R. Long, ''Some aspects of the flow of stratified fluids. A theoretical investigation,'' Tellus **5**, 42 (1953).
[2] R. R. Long, ''Some aspects of the flow of stratified fluids. III. Continuous density gradients,'' Tellus **7**, 341 (1955).
[3] T. L. Clark and W. R. Peltier, ''On the evolution and stability of finite-amplitude mountain waves,'' J. Atmos. Sci. **34**, 1715 (1977).
[4] W. R. Peltier and T. L. Clark, ''The evolution and stability of finite-amplitude mountain waves. Part 2: Surface wave drag and severe downslope windstorms,'' J. Atmos. Sci. **36**, 1498 (1979).
[5] R. Laprise and W. R. Peltier, ''The structure and energetics of transient eddies in a numerical simulation of breaking mountain waves,'' J. Atmos. Sci. **46**, 565 (1989).
[6] P. G. Baines, *Topographic effects in stratified flows* (Cambridge University Press, Cambridge, 1995).
[7] R. B. Smith ''On severe downslope winds,'' J. Atmos. Sci. **42**, 2597 (1985).
[8] R. Laprise and W. R. Peltier, ''The linear stability of nonlinear mountain waves: implications for the understanding of severe downslope windstorms,'' J. Atmos. Sci. **46**, 545 (1989).
[9] Y. D. Afanasyev and W. R. Peltier, ''The three-dimensionalization of stratified flow over two-dimensional topography,'' J. Atmos. Sci. **55**(1), 19 (1998).
[10] G. P. Klassen and W. R. Peltier, ''The onset of turbulence in finite-amplitude Kelvin-Helmholtz billows,'' J. Fluid Mech. **155**, 1 (1985).
[11] D. C. Fritts and J. R. Isler, ''Gravity wave breaking in two and three dimensions 2. Three-dimensional evolution and instability structure,'' J. Geophys. Res. **99**, 8109 (1994).
[12] K. B. Winters and E. A. D'Asaro, ''Three-dimensional wave instability near a critical level,'' J. Fluid Mech. **272**, 255 (1994).
[13] O. Andreassen, P. O. Hvidsten, D. C. Fritts, and S. Arendt, ''Vorticity dynamics in a breaking internal gravity wave. Part 1. Initial instability evolution,'' J. Fluid Mech. **367**, 27 (1998).
[14] P. N. Lombard and J. J. Riley, ''On the breakdown into turbulence of propagating internal waves,'' Dyn. Atmos. Oceans **23**, 345 (1996).
[15] J. W. Rottman and R. B. Smith, ''A laboratory model of severe downslope winds,'' Tellus **41**A, 401 (1989).
[16] I. P. Castro and W. H. Snyder, ''Experiments on wave breaking in stratified flow over obstacles,'' J. Fluid Mech. **225**, 195 (1993).
[17] P. G. Baines and P. C. Manins, ''The principles of laboratory modeling of stratified atmospheric flows over complex terrain,'' J. Appl. Meteorol. **28**, 1213 (1989).
[18] J. C. R. Hunt and W. H. Snyder, ''Experiments on stably and neutrally stratified flow over a model three-dimensional hill,'' J. Fluid Mech. **96**, 671 (1980).
[19] W. H. Snyder, R. S. Thompson, R. E. Eskridge, R. E. Lawson, I. P. Castro, J. T. Lee, J. C. R. Hunt, and Y. Ogawa, ''The structure of strongly stratified flow over hills: dividing-streamline concept,'' J. Fluid Mech. **152**, 249 (1985).
[20] R. Laprise and W. R. Peltier, ''On the structural characteristics of steady finite-amplitude mountain waves over bell-shaped topography,'' J. Atmos. Sci. **46**, 586 (1989).
[21] P. Queney, ''The problem of air flow over mountains: a summary of theoretical studies,'' Bull. Am. Meteorol. Soc. **29**, 16 (1948).
[22] P. Bonneton, O. Auban, and M. Perrier, ''Experiments on two-dimensional lee-wave breaking in stratified flow,'' *Proceedings of IMA conference ''Stably Stratified Flows''* (Dundee, UK, 1996).
[23] S. A. Thorpe, ''Statistically unstable layers produced by overturning internal gravity waves,'' J. Fluid Mech. **260**, 333 (1994).
[24] K. B. Winters and J. J. Riley, ''Instability of internal waves near a critical level,'' Dyn. Atmos. Oceans **16**, 249 (1992).
[25] J. W. Miles, ''On the stability of heterogeneous shear flow,'' J. Fluid Mech. **10**, 496 (1961).
[26] L. N. Howard, ''Note on a paper of John W. Miles,'' J. Fluid Mech. **10**, 509 (1961).
[27] S. I. Voropayev, Y. D. Afanasyev, and G. J. F. van Heijst, ''Experiments on the evolution of gravitational instability of an overturned, initially stably stratified fluid,'' Phys. Fluids A **5**, 2461 (1993).
[28] F. Gheusi, J. Stein, and O. Eiff, ''A numerical study of three-dimensional orographic gravity-wave breaking observed in a hydraulic tank,'' J. Fluid Mech. (to be published).
[29] E. Richard, P. Mascart, and E. C. Nickerson, ''On the role of surface friction in downslope windstorm,'' J. Appl. Meteorol. **28**, 241 (1989).
[30] J. W. Deardorff, ''Gravitational instability between horizontals plates with shear,'' Phys. Fluids **8**(6), 1027 (1965).
[31] G. Tryggvason and S. O. Unverdi, ''Computations of three-dimensional Rayleigh–Taylor instability,'' Phys. Fluids A **2**(5), 656 (1992).
[32] J. W. Jacobs and I. Catton, ''Three dimensional Rayleigh–Taylor instability. Part 1. Weakly nonlinear theory,'' J. Fluid Mech. **587**, 329 (1988).